ACS OMEGA

http://pubs.acs.org/journal/acsodf

Article

CdS Micrometer Hollow Spheres for Detecting Alcohols Except Methanol with Strong Anti-interference Ability

Xueqian Yan, Weiye Yang, Chenyan Li, Lei Liu, and Yingkai Liu*

Cite This: *ACS Omega* 2022, 7, 1468−1476

Read Online

ACCESS | Metrics & More | Article Recommendations

ABSTRACT: Cadmium sulfide micrometer hollow spheres (CdS MHs) were fabricated by a hydrothermal method. The performance of the CdS MHs sensor was evaluated by detecting volatile organic compounds such as methanol, ethanol, 1-propanol, isopropanol, *n*-butanol, *iso*-butyl alcohol, *iso*-amyl alcohol, acetone, and xylene. It was found that the optimum working temperature of the CdS MHs sensor is 190 °C. The response of the CdS MHs can reach 27.4−100 ppm ethanol and reach 84.55−100 ppm isopropanol. Comparing the response to pure 5 ppm isopropanol (*iso*-amyl alcohol) with the mixture of 5 ppm isopropanol (*iso*-amyl alcohol) and 50 ppm acetone or 5 ppm isopropanol (*iso*-amyl alcohol) and 50 ppm methanol, the relative deviation was −1.33% (−7.11%) or −6.19% (9.20%). It suggested that the CdS MHs sensor had a strong anti-interference ability to methanol and acetone and is suitable for detecting alcohols except methanol. Therefore, the CdS MHs sensor had good response and is a promising alcohol detection material.

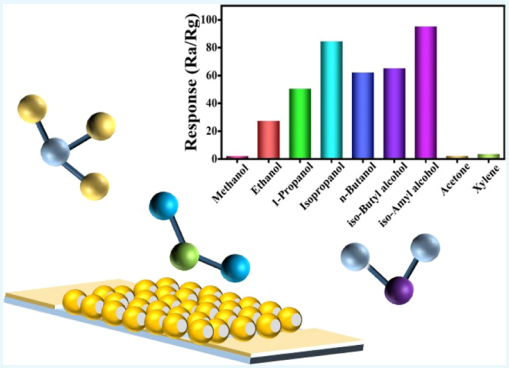

1. INTRODUCTION

In the modern society, the rapid development of industrialization continues to improve people's living standards, but it also emits various harmful gases including acetone,[1] toluene,[2] hydrogen sulfide,[3] isopropanol,[4] nitric oxide,[5] nitrogen dioxide,[6] and so on. There is a huge demand for high performance gas sensors. Generally, most of them are made of metal oxide semiconductors (MOS) such as tin dioxide,[7] zinc oxide,[8] copper oxide,[9] and titanium dioxide,[10] and so forth. A MOS gas sensor is the fastest development and widely used gas sensor. Especially, tin dioxide has been the hotspot of gas sensors. Kim[11] et al. reported that In^{3+} ions were implanted into SnO_2 nanowires to produce a uniform homo-core shell (C−S) structure and revealed that ion implantation can promote its sensing detective capability. Of course, not only tin oxide, other oxides also have excellent performance, such as low temperature ammonia sensor based on p-type MoS_2 nanoparticle modified Cu_2O nanoparticles.[12] Meanwhile, it is found that the sensitivity and selectivity of the sensor are related to the structure, morphology[13] and composition of its based material such as doped noble metals,[11] heterojunction structure[14] (n−n junctions structure and n−p junctions structure), and defects. The defects have an influence on response, sensitivity, and response/recovery time. The more surface defects, the stronger the influence[15] is.

However, metal sulfides are less studied for gas detection. Cadmium sulfide is a kind of metal sulfide and a typical semiconductor material. It has two types of phase structures, that is, wurtzite and zinc blende. It is found that cadmium sulfide changed from zinc blende to wurtzite[16] as its nanocrystal size increases. Cadmium sulfide with various morphologies such as nanoflowers,[17] nanoribbons,[18] and nanosheets (NSs)[19] were synthesized by chemical vapor deposition, hydrothermal method, and sol−gel method, and so forth. At present, cadmium sulfide has been widely used in the fields of photocatalysis degradation of organic pollutants,[20] optoelectronic devices,[21] surface-enhanced Raman spectroscopy detection,[17] and solar cells.[22] At the same time, CdS is also a good candidate for gas sensors. Zhang et al. prepared a CdS nanorods growing on a polyaniline-Cd^{2+} particles surface (CdS/PANI) that showed good response to low concentrations of formaldehyde gas over a wide temperature range of 80−140 °C.[23] Bai et al. synthesized a novel mesoporous heterostructure (CdS/PbS/SnO_2) composed of CdS, PbS, and SnO_2, which has excellent selectivity for H_2 gas, reliable reversibility and 40 days long-term stability.[24] CdS combines with other materials to form highly efficient heterogeneous structures in gas sensors. Srinivasan and Jeyaprakash investigated the spray deposited ZnO/CdS heterostructures, which show remarkable advantages for formaldehyde vapors

Received: November 4, 2021
Accepted: December 17, 2021
Published: December 28, 2021

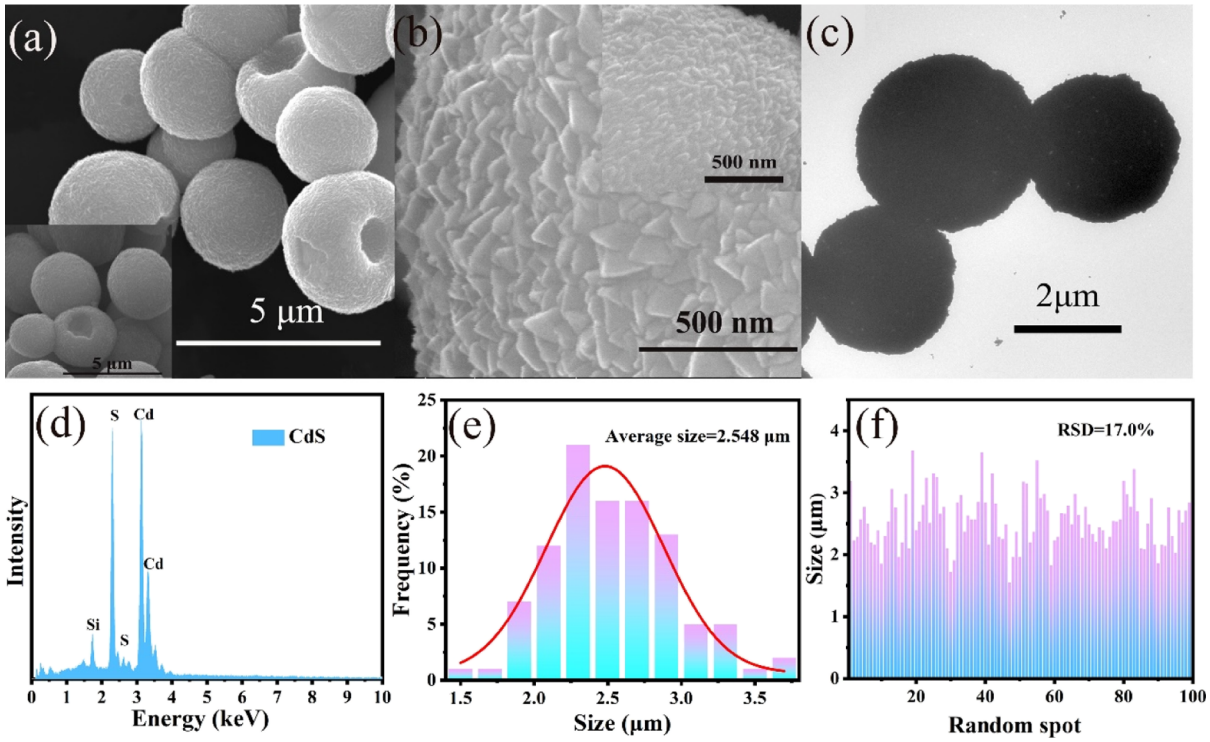

Figure 1. SEM, TEM, EDS, and particle size analysis images of CdS MHs (a,b) SEM images at low/high magnification, inset: SEM images after sensing measurement; (c) TEM; (d) EDS; (e) statistical histogram; (f) standard deviation.

under the action of room temperature photons. The minimum detection limit of formaldehyde is 10 ppm. The response time to 10 ppm formaldehyde is 78 s and recovery time is 25 s, which is better than pure cadmium sulfide and zinc oxide.[25] Herein, we prepared cadmium sulfide micrometer hollow spheres (MHs) and studied their sensing properties. It revealed that CdS MHs were more sensitive to alcohols except for methanol than ketones and benzene. In the mixed solution of alcohol with methanol and acetone, it exhibited an excellent response to alcohol with strong anti-interference ability.

2. RESULT AND DISCUSSION

2.1. Morphological, Structural, and Compositional Properties of CdS MHs. Figure 1a shows a SEM image of CdS MHs. It is clearly seen that the CdS MHs with average diameter of 2−3 μm have deep holes in the middle of them. It further revealed that its surface is rough. From its image with large magnification (Figure 1b), we can see that the CdS MHs are self-assembled from CdS NSs. The insets of Figure 1a,b show the morphology of cadmium sulfide after sensing measurement, further indicating that the active layer of cadmium sulfide has not changed. The corresponding transmission electron microscopy (TEM) image is shown in Figure 1c. Small spheres with a diameter of about 2 μm can be clearly observed. In order to determine their composition, we performed energy dispersive X-ray spectroscopy (EDS) analysis of them, as displayed in Figure 1d. They are composed of Cd and S elements. The Si signal comes from silicon substrate. The element composition calculated by EDS analysis is 23.53 wt % of S, 73.86 wt % of Cd, and 2.63 wt % of Si. The content of Cd, S, and Si elements are 44.28, 49.46, and 6.26 at. %, respectively. EDS quantitative analysis of the stoichiometric ratio of Cd to S is about 1:1. This means that the elements of Cd and S form CdS. Figure 2e,f shows the diameter

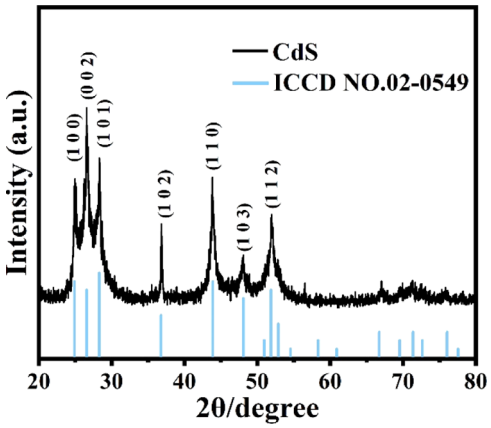

Figure 2. XRD pattern of CdS MHs.

distribution of random CdS MHs. It can be seen that the average width of CdS MHs is 2.548 μm in Figure 2e. The standard deviation is about 17.0%, indicating that the size of CdS MHs is relatively uniform, as shown in Figure 2f.

Figure 2 describes the XRD pattern of CdS MHs. It presented that all diffraction peaks were consistent with hexagonal wurtzite CdS with $a = b = 4.142$ Å, $c = 6.72$ Å [ICDD (International Center of Diffraction Data) no. 02-0549]. The 2θ located at 25.10°, 26.54°, 28.18°, 36.84°, 43.85°, 47.29° and 52.05°, corresponding to the (1 0 0), (0 0 2), (1 0 1), (1 0 2), (1 1 0), (1 0 3), and (1 1 2) crystal planes, respectively. The strong and sharp peaks unraveled that CdS MHs have good crystallinity. The XRD pattern showed that no other impurities were detected.

X-ray photoelectron spectroscopy (XPS) is conducted to explore the surface element composition and chemical state of the CdS MHs. Figure 3a shows the full-scan XPS spectrum of

https://doi.org/10.1021/acsomega.1c06211
ACS Omega 2022, 7, 1468−1476

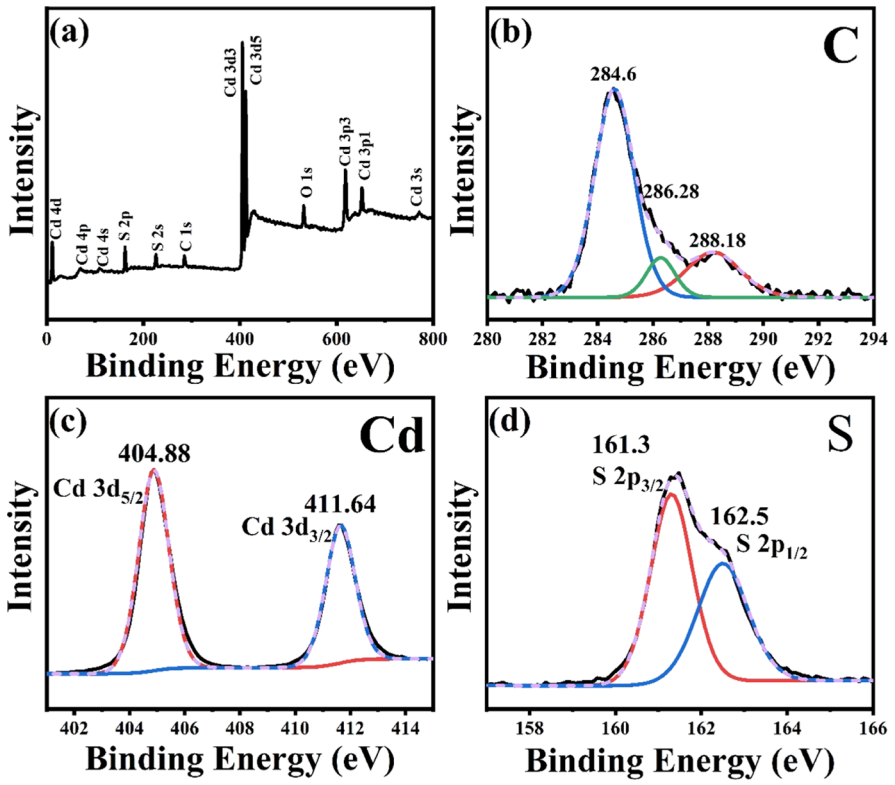

Figure 3. XPS analysis of the CdS MHs (a) The full XPS spectrum; (b) C region; (c) Cd region; (d) S region.

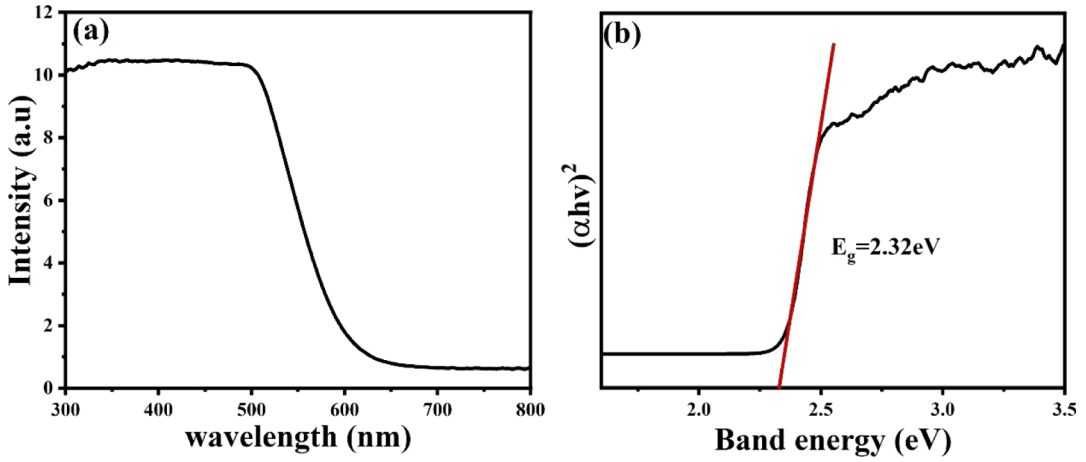

Figure 4. (a) UV−vis absorption spectrum of CdS MHs; (b) relationship between $(\alpha h\nu)2$ and photonic energy $h\nu$ of CdS MHs.

CdS. It indicates that the sample is composed of Cd, S, C, and O elements. The presence of oxygen is due to oxygen ions adsorbed on the surface of the sample. The C 1s spectrum in Figure 3b has three peaks at the binding energies of 284.6, 286.28, and 288.18 eV. The peak of C 1s at 284.6 eV was used as a standard to calibrate the binding energy in the XPS. As can be seen from Figure 3c, Cd 3d spectra have two peaks with a distance of 6.8 eV.[26] One is at 411.64 eV and the other is at 404.88 eV, representing the electronic states of Cd $3d_{3/2}$ and Cd $3d_{5/2}$ respectively. The peak of S 2p is exposed in Figure 3d, and the binding energies of S $2p_{3/2}$ and S $2p_{1/2}$ were 161.3 and 162.5 eV, respectively.

It is seen from Figure 4a that the CdS MHs has a wide absorption in the range of 300−500 nm with absorption edge of 500 nm. Its optical band gap is calculated by the following formula

$$\alpha h\nu = A(h\nu - E_g)^{1/n} \quad (1)$$

For direct band gap semiconductor, n is equal to 2. The optical band gap (E_g) of the CdS MHs is 2.32 eV, being smaller than that of the bulk CdS (2.42 eV), as shown in Figure 4b. It suggests that nanoparticles have an effect on narrowing the band gap.

2.2. Gas Sensing Performance of CdS MHs. The response of gas sensor was greatly affected by the operating temperature, which was widely calculated by eq 2.

$$S = \frac{R_a}{R_g} \quad (2)$$

https://doi.org/10.1021/acsomega.1c06211
ACS Omega 2022, 7, 1468−1476

where S was gas response, R_g was the electrical resistance either in the mixture gas or target gas, and R_a was the baseline electrical resistance of the gas sensor in air.

Figure 5 exposes the gas-sensitive response of the CdS MHs to 100 ppm isopropanol and ethanol at 160−230 °C. All

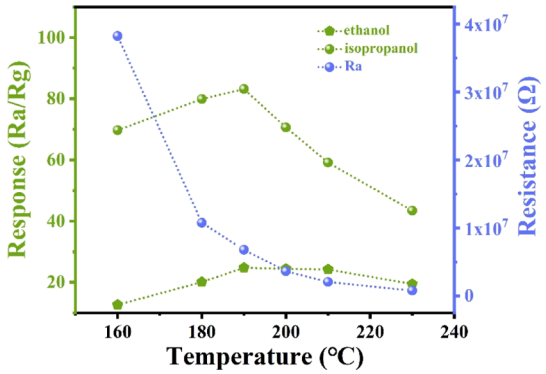

Figure 5. Response of the gas sensor based on CdS MHs toward 100 ppm isopropanol and ethanol at different working temperatures.

measurements were made at around 48% relative humidity. The response increases with temperature, but decreases with the increment of temperature after 190 °C. Moreover, the initial resistance (R_a) decreases with the increase of operating temperature. Therefore, its optimum working temperature is at 190 °C.

Figure 6 shows the response curves of CdS MHs versus concentration within the scope of 10−1000 ppm to different

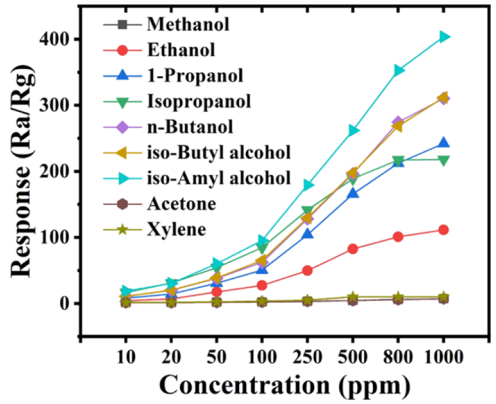

Figure 6. Response of CdS MHs versus concentration in the range of 10−1000 ppm toward different organics volatile gases including methanol, ethanol, 1-propanol, isopropanol, *n*-butanol, *iso*-butyl alcohol, *iso*-amyl alcohol, acetone, and xylene at 190 °C.

organic volatile gases. The response of gas sensor is affected by gas concentration. In addition, when the concentration of isopropanol is high, it shows a saturation state. The response dependence on gas concentration is also studied. Figure 7 shows the fitting curves versus concentration of ethanol, 1-propanol, isopropanol, *n*-butanol, *iso*-butyl alcohol, and *iso*-amyl alcohol at 10−250 ppm, indicating that the response is significantly dependent on the concentration. The fitting line equations and their correlated coefficients (R^2) are listed in Table 1. The R^2 approach 1, indicating the stronger the correlation between the two variables, the better the regression.

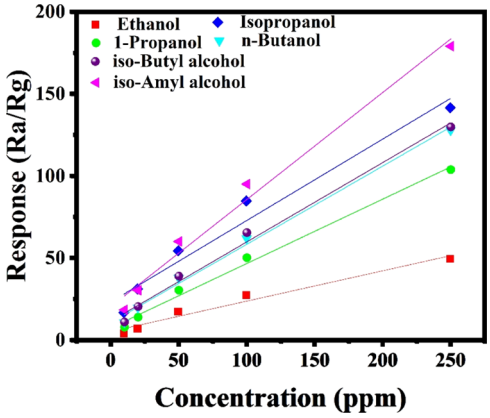

Figure 7. Fitted lines of the response versus concentration to six alcohols including methanol, ethanol, 1-propanol, isopropanol, *n*-butanol, *iso*-butyl alcohol, and *iso*-amyl alcohol at 190 °C.

Table 1. Fitted Parameters and LOD Values of the CdS MHs toward Six Kinds of Alcohols

target gas	the linear relationship	R^2	LOD/ppb
ethanol	$Y = 0.18479x + 5.20831$	0.97183	98
1-propanol	$Y = 0.49629x + 22.86864$	0.96463	34
isopropanol	$Y = 0.39241x + 7.71896$	0.99320	13
n-butanol	$Y = 0.47648x + 10.78039$	0.99416	11
iso-butyl alcohol	$Y = 0.48345x + 11.29624$	0.99141	14
iso-amyl alcohol	$Y = 0.65235x + 20.62376$	0.98552	18

One of its important parameters is the theoretical limit of detection (LOD), which was received by the signal-to-noise ratio. Furthermore, the root mean square deviation (rms) was used to reveal the response change of the sensor and then the continuous 40 points were selected to do it. The LOD is calculated by eqs 3−5.[27,28]

$$V_{\chi^2} = \sum (y_i - y)^2 \tag{3}$$

$$\mathrm{rms}_{\mathrm{noise}} = \sqrt{\frac{V_{\chi^2}}{N}} \tag{4}$$

$$\mathrm{LOD(ppm)} = 3\frac{\mathrm{rms}}{\mathrm{slope}} \tag{5}$$

where y_i was the experimentally measured data, y was the corresponding calculated results by the fifth-order polynomial fitting of the measured data, and N was the number of data points. The fitted lines of response versus concentration are displayed in Figure 7. For instance, the V_{χ^2} and N of isopropanol are 0.00129 and 40, respectively. The noise of the sensor is evaluated to be 0.005678 and the slope is 0.49629. Therefore, the LOD of the isopropanol is 34 ppb. For other gases, their corresponding results are also listed in Table 1. It is seen that the LODs are less than 100 ppb for the measured six alcohols.

Figure 8 is a bar diagram of the CdS MH sensors responding to different organic gases at 190 °C. In detail, the response of it are 2.18, 3.519, 2.038, 27.4, 50.393, 84.55, 62.109, 65.173, and 95.2−100 ppm of acetone, xylene, methanol, ethanol, 1-propanol, isopropanol, *n*-butanol, *iso*-butanol alcohol, and *iso*-amyl alcohol, respectively. In contrast to ketones and benzenes, it revealed that the CdS MHs sensor is sensitive to alcohols

https://doi.org/10.1021/acsomega.1c06211
ACS Omega 2022, 7, 1468−1476

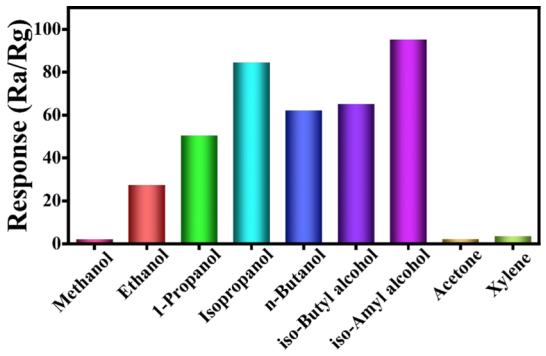

Figure 8. Bar diagram of CdS MHs sensor responding to 100 ppm of different organic gases at 190 °C.

except methanol. In short, the device has good selectivity to alcohols.

In order to explore the anti-interference capability of the CdS MHs sensor to acetone and methanol, its response to 5 ppm isopropanol (*iso*-amyl alcohol) is measured under the interference of 50 ppm acetone methanol, respectively. The results are denoted in Figure 9. It is very stable for CdS MHs sensor to monitor 5 ppm isopropanol (*iso*-amyl alcohol). Comparing the response to pure 5 ppm isopropanol (*iso*-amyl alcohol) with the mixture of 5 ppm isopropanol (*iso*-amyl alcohol) and 50 ppm acetone or 5 ppm isopropanol (*iso*-amyl alcohol) and 50 ppm methanol, the relative deviation is −1.33% (−7.11%) or −6.19% (9.20%). Similarly, for ethanol, the relative deviation is −13.5 or −4.55%, as shown in Figure 9. Our CdS MHs sensor has strong anti-interference ability to methanol and acetone. Therefore, it is suitable for sensing alcohols except methanol and especially exhibits superior performance on detecting isopropanol.

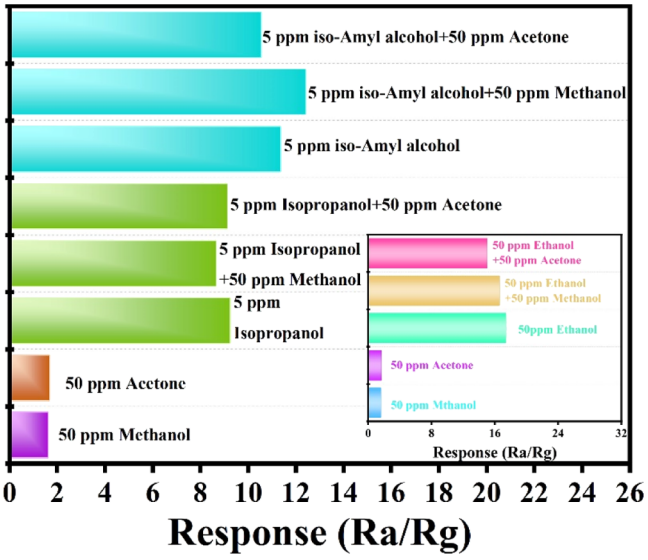

Figure 9. Histogram of the sensitive response to 5 ppm isopropanol and *iso*-amyl alcohol under the background of 50 ppm of different interference gases at 190 °C.

In order to further delve its application feasibility to monitor drunk driving, the repeatability of the sensor to 100 ppm ethanol was examined. The CdS MHs sensor was also undergone gas-sensing tests for 24 days, as shown in Figure 10a. It is found that the response to 100 ppm ethanol maintained around 27.4 although it had some faint fluctuation. These results revealed that the CdS MHs sensor had potential for monitoring ethanol with long-time stability. Figure 10b shows the rise time and fall time of 100 ppm ethanol response at 190 °C. The response time is defined as the time it takes for the sensor resistance under the gas to be measured to move from the reference value to 90% of the resistance value. Similarly, recovery time is the time it takes for the device to fall from its maximum response value to 10% of its maximum response value. In the figure, the rise time is 38 s and the fall time is 4 s.

The reported ethanol and isopropanol sensing properties of various morphologies sensors were compared with the above-prepared CdS MHs sensors, as recorded in Table 2. It was found that the CdS MHs sensor has achieved better performance toward ethanol and isopropanol gas at lower working temperatures, disclosing that it possess great feasibility in detecting alcohols except methanol.

2.3. Sensing Mechanism. The sensing mechanism may be the adsorption and desorption of target molecules on the surface of the material,[36] resulting in the resistance change. The surface of the device adsorbs oxygen molecules in air, which are affected by temperature and surface conditions. Then, oxygen molecules form three types of oxygen ions[37] such as O_2^-, O^-, and O^{2-}. Cadmium sulfide is an n-type semiconductor. Adsorbed oxygen molecules cause electrons to transfer from the conduction band to the sensor surface. With the presence of the electron depletion layer, the resistance increases.[38] The reaction equation was as follows[39]

$$O_2 + e^- \rightarrow O_2^- \qquad (T < 100\ ^\circ C) \tag{6}$$

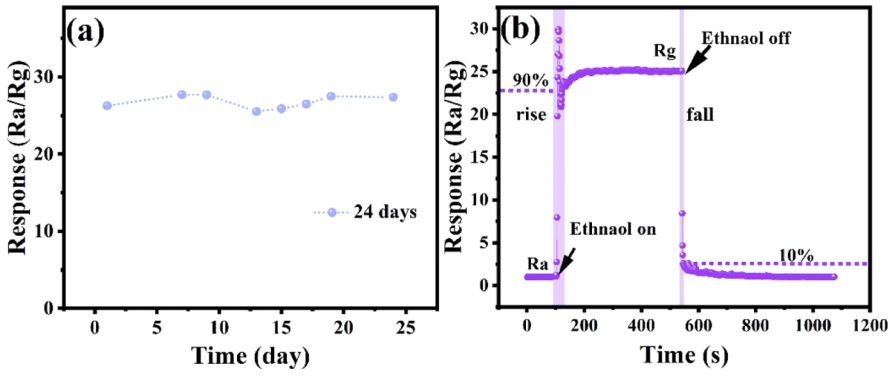

Figure 10. 100 ppm ethanol on CdS MHs gas sensor at 190 °C. (a) Response stability. (b) Time of rise and time of descent.

https://doi.org/10.1021/acsomega.1c06211
ACS Omega 2022, 7, 1468−1476

Table 2. Comparison of the Sensing Performances Based on Different Mophology of CdS

sensing material	target gas	operating temperature (°C)	concentration (ppm)	response	refs
NUM-CdS-3	ethanol	230	100	20	29
CdS nanowires	ethanol	206	100	14.9	30
TiO_2 pellets	ethanol	300	1000	12.32	31
Au−CuO	ethanol	160	500	8.6	32
CdS nanoflakes	isopropanol	225	200	76	33
CdS leaf-like	isopropanol	210	100	63	34
SnO_2 nanorings	isopropanol	250	100	7.27	35
CuO−SnO_2 nanorods	isopropanol	280	100	50.4	4
CdS micron hollow sphere	isopropanol	190	100	84.55	this study
CdS micron hollow sphere	ethanol	190	100	27.4	this study

$$O_2^- + e^- \rightarrow 2O^- \quad (100\ ^\circ C < T < 300\ ^\circ C) \tag{7}$$

$$O^- + e^- \rightarrow O^{2-} (T > 300) \tag{8}$$

The specific determination of the type of oxygen ions is defined as by eq 9[40]

$$S = 1 + aC^b \tag{9}$$

Equation 9 can be expressed as

$$\log(S-1) = b\ \log C + \log a \tag{10}$$

where S represents the response of the target gas, and C is the corresponding gas concentration. Both "a" and "b" are constants, which are fitted from experimental data and represent the prefactor and charge parameters. The fitting line of $\log(S-1)$ versus $\log C$ is displayed in Figure 11 and

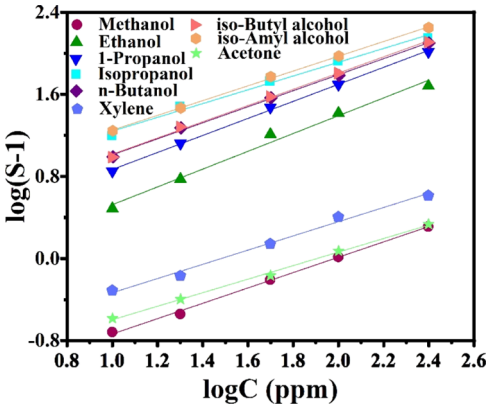

Figure 11. $\log(S-1)$ vs $\log C$ for CdS gas sensors at 190 °C.

the fitted equations to all target gases are summarized in Table 3. It is observed that the $\log(S-1)$ versus $\log C$ of our sensor

Table 3. Fitted Linear Equations of $\log(S-1)$ vs $\log C$ for all the Target Gases

target gas	the fitted linear equations	b
methanol	$\log(S-1) = 0.74829 \log C - 1.48442$	0.74829
ethanol	$\log(S-1) = 0.86761 \log C - 0.33874$	0.86761
1-propanol	$\log(S-1) = 0.83004 \log C + 0.03544$	0.83004
isopropanol	$\log(S-1) = 0.67141 \log C + 0.56536$	0.67141
n-butanol	$\log(S-1) = 0.78115 \log C + 0.23328$	0.78115
iso-butyl alcohol	$\log(S-1) = 0.79098 \log C + 0.22409$	0.79098
iso-amyl alcohol	$\log(S-1) = 0.75021 \log C + 0.53261$	0.75021
acetone	$\log(S-1) = 0.65999 \log C - 0.25742$	0.65999
xylene	$\log(S-1) = 0.69267 \log C - 1.03095$	0.69267

to all target gases show a good linear increment. The state of oxygen ions is determined by b. The surface adsorption is O^- when b is 1 and the surface adsorption is O^{2-} while b is equal to 0.5. The charge parameter of all target gases are between 0.5 and 1, indicating that O^- and O^{2-} coexist. For alcoholic gases, there are many O^{2-} ions, and the response may be good. It may be that O^{2-} is more unstable than O_2^- and O^- and has stronger energy.[41]

In contrast, the gas will be adsorbed on the surface of the sensor as the n-type CdS MHs sensor was exposed to the target gas. These alcohols gases will react with the chemically adsorbed oxygen to produce water and carbon dioxide. The charge layer at the surface is already a depletion layer due to the adsorption of oxygen. The electrons are released back to the material of cadmium sulfide, and finally the depletion layer thickness on the surface of the sensor will be decrease, and decrease in surface band bending, resulting in resistance decrease.[38] The react formulae for several target gases can be expressed as eqs 11−19[42−45]

$$CH_3OH + O^{2-} \rightarrow HCHO + H_2O + 2e^- \tag{11}$$

$$CH_3CH_2OH + 6O^- \rightarrow 2CO_2 + 3H_2O + 6e^- \tag{12}$$

$$CH_3CH_2CH_2OH + 9O^- \rightarrow 3CO_2 + 4H_2O + 9e^- \tag{13}$$

$$(CH_3)_2CHOH + 9O^{2-} \rightarrow 3CO_2 + 4H_2O + 18e^- \tag{14}$$

$$CH_3CH_2CH_2CH_2OH + 12O^- \rightarrow 4CO_2 + 5H_2O + 12e^- \tag{15}$$

$$CH_3CH(CH_3)CH_2OH + 12O^- \rightarrow 4CO_2 + 5H_2O + 12e^- \tag{16}$$

$$C_5H_{12}O + 15O^- \rightarrow 5CO_2 + 6H_2O + 15e^- \tag{17}$$

$$CH_3COCH_3 + O^{2-} \rightarrow CH_3C^+O + CH_3O^- + 2e^- \tag{18}$$

$$C_6H_4CH_3CH_3 + 2O^{2-} \rightarrow C_6H_4CH_3CHO + H_2O + 4e^- \tag{19}$$

Based on the previous theory, the gas-sensitive response of alcohols is proportional to the length of the carbon chain.[46] Here, we found through experiments that isopropanol has an abnormally high response, which may be due to its different molecular structures. In the reaction, the alcohol takes off the H and oxygen ions to form water molecules. Methanol molecule dehydrogenates from the $-CH_3$ group, while isopropanol dehydrogenates from the −CH group. The bond energy of −CH is lower than that of $-CH_3$ and the electronegativity is weak, so isopropanol can have a strong

https://doi.org/10.1021/acsomega.1c06211
ACS Omega 2022, 7, 1468−1476

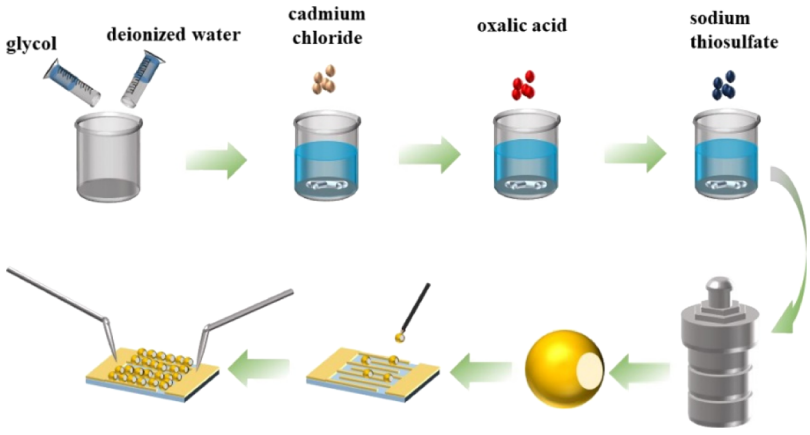

Figure 12. Diagram of CdS preparation and test.

response. All the other alcohols are $-CH_2$, which is the chain principle.

3. CONCLUSIONS

Cadmium sulfide MHs prepared by the hydrothermal method were analyzed by XRD, XPS, TEM, SEM, and EDS to explore its microscopic morphology, compositions, and microstructures. The response of the CdS MHs sensor is 2.18/3.519/2.038/27.4/50.393/84.55/62.109/65.173/95.2−100 ppm of acetone/xylene/methanol/ethanol/1-propanol/isopropanol/*n*-butanol/*iso*-butanol alcohol/*iso*-amyl alcohol, respectively, at 190 °C. In contrast to ketones and benzenes, it revealed that the CdS MHs are sensitive to alcohols except methanol. Accordingly, the theoretical LOD values are 98, 34, 13, 11, 14, and 18 ppb for ethanol, 1-propanol, isopropanol, *n*-butanol, *iso*-butyl alcohol, and *iso*-amyl alcohol, respectively. The CdS MH sensors have achieved excellent performance on the mixed organic gases of alcohols and methanol, alcohols, and acetone, suggesting that they own outstanding anti-interference capability to methanol and acetone.

4. EXPERIMENTAL SECTION

4.1. Materials. Cadmium chloride, glycol, oxalic acid, sodium thiosulfate, methanol, 1-propanol, isopropanol, and xylene were purchased from Tianjin Fengchuan Chemical Reagent Technologies Co., Ltd. Ethanol absolute and *n*-butanol were bought from Tianjin Zhiyuan Chemical Reagent Co., Ltd. Acetone was obtained from Yunnan Yanglin Industrial Development Zone Shandian Pharmaceutical Co., Ltd. *Iso*-amyl alcohol and *iso*-butyl alcohol were bought from Tianjin Jingdong Tianzheng Precision Chemical Reagent Factory. Experimental materials were of analytical grade and did not undergo further treatment.

4.2. CdS MHs Preparation. The synthesis of the CdS MHs were executed by a simple hydrothermal method, which was followed on the previously reported literature.[47] First, 0.008 mol of cadmium chloride was poured into 24 mL of glycol and 40 mL of deionized water (the ratio of glycol to deionized water is 3:5). Then, add 0.008 mol of oxalic acid and 0.016 mol of sodium thiosulfate in turn. After stirring 30 min, the aforementioned solution was transferred into Teflon lined stainless autoclave, raised up to 120 °C and maintained at this temperature for 24 h. After the reaction, the product naturally cooled to room temperature and was washed and centrifuged with deionized water and absolute ethanol. Finally, the product was dried in an oven at 60 °C for 12 h. Thus, CdS MHs were obtained. Because CdS NSs self-assemble into small spheres during the reaction process. However, these balls have high energy. In order to maintain the energy balance of the system, coupled with the hexagonal structure of CdS, each CdS ball forms a pit along the c axis and releases part of the energy. In the end, the pits continue to deepen and form a CdS micron hollow structure.

4.3. Measurement. The sensor was fabricated as follows: First, the gold fork electrode was treated by a plasma cleaning machine for 2 min so that it was convenient for the subsequent coating paste. Next, mix the sample and water with a ratio of 1:150 into the agate mortar and gently ground into pulp. After that, the paste was coated onto the gold interdigital electrode substrate by a paint pen. The electrode spacing is about 1 mm, the electrode wire width is 1 mm, the electrode sheet size is about 15 mm × 10 mm, and the sensor layer thickness is about 120 μm. Thus, the sensor is attained. Finally, let the coated substrate age for 48 h at 190 °C. Thus, the sensor is ready for test. The morphology of CdS MHs remained the same after 48 h of aging. The sensing measurement is carried out by a CGS-1TP Intelligent Gas Sensing Analysis System (Beijing Elite Tech Co., Ltd). A simple experiment and device preparation flow chart is shown in Figure 12.

Gas response measurement procedure is as follows: (1) the prepared device is placed on the test platform of CGS-1TP Intelligent Gas Sensing Analysis System (Beijing Elite Tech Co., Ltd). (2) the cover is closed to form a closed system after the probe is pricked on the gold electrode to form a loop. (3) A certain amount of volatile organic compounds (VOCs) is injected into the evaporation tray to make it evaporate. In this environment, the resistance of the sensor varies with VOC gas concentration change. Finally, the lid of the chamber was removed for desorption after the measurement was finished.

4.4. Characterization. The morphology and microstructures of the CdS MHs were considered by scanning electron microscopy (SEM, Quanta FEG 250, America) and TEM (JEOL 2010, Japan). UV−vis absorption spectra of the CdS MHs were measured by an ultraviolet/visible/near infrared spectrophotometer (U-4100, Japan). The crystalline structure of the sample was identified by X-ray diffractometry (XRD, D/MAX-3B Rigaku, Japan) with Cu Kα_1 radiation (λ = 1.5406 Å, 2θ = 20−100°). XPS (K-Alpha+, America) was performed to analyze the binding states between valence electrons of the CdS samples.

https://doi.org/10.1021/acsomega.1c06211
ACS Omega 2022, 7, 1468−1476

AUTHOR INFORMATION

Corresponding Author

Yingkai Liu − *Yunnan Key Laboratory of Opto-Electronic Information Technology, Yunnan Normal University, Kunming 650500, China; Institute of Physics and Electronic Information and Key Laboratory of Advanced Technique & Preparation for Renewable Energy Materials, Ministry of Education, Yunnan Normal University, Kunming 650500, China*; Phone: +86-871-6594-1166; Email: ykliu@ynnu.edu.cn

Authors

Xueqian Yan − *Yunnan Key Laboratory of Opto-Electronic Information Technology, Yunnan Normal University, Kunming 650500, China; Institute of Physics and Electronic Information, Yunnan Normal University, Kunming 650500, China*; orcid.org/0000-0002-2254-3642

Weiye Yang − *Yunnan Key Laboratory of Opto-Electronic Information Technology, Yunnan Normal University, Kunming 650500, China; Institute of Physics and Electronic Information, Yunnan Normal University, Kunming 650500, China*; orcid.org/0000-0001-5685-5727

Chenyan Li − *Yunnan Key Laboratory of Opto-Electronic Information Technology, Yunnan Normal University, Kunming 650500, China; Institute of Physics and Electronic Information, Yunnan Normal University, Kunming 650500, China*

Lei Liu − *Yunnan Key Laboratory of Opto-Electronic Information Technology, Yunnan Normal University, Kunming 650500, China; Institute of Physics and Electronic Information, Yunnan Normal University, Kunming 650500, China*

Complete contact information is available at: https://pubs.acs.org/10.1021/acsomega.1c06211

Notes

The authors declare no competing financial interest.

ACKNOWLEDGMENTS

The research was provided by the National Natural Science Foundation of China (grant nos. 11764046, 11764047).

REFERENCES

(1) Cheng, P.; Lv, L.; Wang, Y.; Zhang, B.; Zhang, Y.; Zhang, Y.; Lei, Z.; Xu, L. $SnO_2/ZnSnO_3$ double-shelled hollow microspheres based high-performance acetone gas sensor. *Sens. Actuators, B* **2021**, *332*, 129212.

(2) Ueda, T.; Abe, H.; Kamada, K.; Bishop, S. R.; Tuller, H. L.; Hyodo, T.; Shimizu, Y. Enhanced sensing response of solid-electrolyte gas sensors to toluene: Role of composite Au/metal oxide sensing electrode. *Sens. Actuators, B* **2017**, *252*, 268−276.

(3) Chen, J.; Guo, L.; Chen, L.; Qiu, B.; Hong, G.; Lin, Z. Sensing of Hydrogen Sulfide Gas in the Raman-Silent Region Based on Gold Nano-Bipyramids (Au NBPs) Encapsulated by Zeolitic Imidazolate Framework-8. *ACS Sens.* **2020**, *5*, 3964−3970.

(4) Zhang, B.; Fu, W.; Meng, X.; A, R.; Su, P.; Yang, H. Synthesis of actinomorphic flower-like SnO_2 nanorods decorated with CuO nanoparticles and their improved isopropanol sensing properties. *Appl. Surf. Sci.* **2018**, *456*, 586−593.

(5) Qiu, J.; Hu, X.; Min, X.; Quan, W.; Tian, R.; Ji, P.; Zheng, H.; Qin, W.; Wang, H.; Pan, T.; Cheng, S.; Chen, X.; Zhang, W.; Wang, X. The observation of switchable dual conductive channels and related nitric oxide gas sensing properties in N-rGO/ZnO heterogeneous structure. *ACS Appl. Mater. Interfaces* **2020**, *12*, 19755−19767.

(6) Zhou, Y.; Yw, A.; Yw, A.; Xian, L. B.; Yg, A. The impact of carrier gas on room-temperature trace nitrogen dioxide sensing of ZnO nanowire-integrated film under UV illumination. *Ceram. Int.* **2020**, *46*, 16056−16061.

(7) Wang, Y.-Y.; Na, H.-B.; Zhang, M.; Deng, Z.-P.; Huo, L.-H.; Gao, S. Coca-Cola solvothermal synthesis of mesoporous SnO_2 blooming flower-like architecture assembled from single crystal nanorods and its gas sensing properties. *Powder Technol.* **2020**, *375*, 463−471.

(8) Cheng, I.-K.; Lin, C.-Y.; Pan, F.-M. Gas sensing behavior of ZnO toward H_2 at temperatures below 300°C and its dependence on humidity and Pt-decoration. *Appl. Surf. Sci.* **2021**, *541*, 148551.

(9) Qiang, H. A.; Wz, A.; Xw, A.; Qiao, W. A.; Bh, B.; Yan, L. A.; Xh, A.; Guo, L. A.; Bl, C.; Jz, A. Binder-free CuO nanoneedle arrays based tube-type sensor for H_2S gas sensing. *Sens. Actuators, B* **2020**, *326*, 128993.

(10) Wang, M.; Jin, C.; Luo, Q.; Kim, E. J. Sol-gel derived TiO_2−carbon composites with adsorption-enhanced photocatalytic activity and gas sensing performance. *Ceram. Int.* **2020**, *46*, 18608−18613.

(11) Kim, J.-H.; Kim, J.-Y.; Lee, J.-H.; Mirzaei, A.; Kim, H. W.; Hishita, S.; Kim, S. S. Indium-implantation-induced enhancement of gas sensing behaviors of SnO_2 nanowires by the formation of homo-core−shell structure. *Sens. Actuators, B* **2020**, *321*, 128475.

(12) Ding, Y.; Guo, X.; Du, B.; Hu, X.; Yang, X.; He, Y.; Zhou, Y.; Zang, Z. Low-operating temperature ammonia sensor based on Cu_2O nanoparticles decorated with p-type MoS_2 nanosheets. *J. Mater. Chem. C* **2021**, *9*, 4838−4846.

(13) Wan, X.; Wang, J.; Zhu, L.; Tang, J. Gas sensing properties of Cu_2O and its particle size and morphology-dependent gas-detection sensitivity. *J. Mater. Chem. A* **2014**, *2*, 13641−13647.

(14) Liu, Y.; Hao, L.; Gao, W.; Wu, Z.; Lin, Y.; Li, G.; Guo, W.; Yu, L.; Zeng, H.; Zhu, J.; Zhang, W. Hydrogen gas sensing properties of MoS_2/Si heterojunction. *Sens. Actuators, B* **2015**, *211*, 537−543.

(15) Choi, P. G.; Fuchigami, T.; Kakimoto, K.-i.; Masuda, Y. Effect of Crystal Defect on Gas Sensing Properties of Co_3O_4 Nanoparticle. *ACS Sens.* **2020**, *5*, 1665−1673.

(16) Nag, A.; Hazarika, A.; Shanavas, K. V.; Sharma, S. M.; Dasgupta, I.; Sarma, D. D. Crystal Structure Engineering by Fine-Tuning the Surface Energy: The Case of CdE (E = S/Se) Nanocrystals. *J. Phys. Chem. Lett.* **2011**, *2*, 706−712.

(17) Yang, C.; Qing, C.; Wang, Q.; Zhang, X.; Lou, J.; Liu, Y. Synthesis of the hybrid CdS/Au flower-like nanomaterials and their SERS application. *Sens. Actuators, B* **2020**, *304*, 127218.

(18) Pan, A.; Liu, D.; Liu, R.; Wang, F.; Zhu, X.; Zou, B. Optical Waveguide through CdS Nanoribbons. *Small* **2005**, *1*, 980−983.

(19) Xu, Y.; Zhao, W.; Xu, R.; Shi, Y.; Zhang, B. Synthesis of ultrathin CdS nanosheets as efficient visible-light-driven water splitting photocatalysts for hydrogen evolution. *Chem. Commun.* **2013**, *49*, 9803−9805.

(20) Liu, Y.; Shen, S.; Zhang, J.; Zhong, W.; Huang, X. $Cu_{2-x}Se$/CdS composite photocatalyst with enhanced visible light photocatalysis activity. *Appl. Surf. Sci.* **2019**, *478*, 762−769.

(21) Ye, Y.; Dai, L.; Wen, X.; Wu, P.; Pen, R.; Qin, G. High-Performance Single CdS Nanobelt Metal-Semiconductor Field-Effect Transistor-Based Photodetectors. *ACS Appl. Mater. Interfaces* **2010**, *2*, 2724−2727.

(22) Ye, Y.; Dai, Y.; Dai, L.; Shi, Z.; Liu, N.; Wang, F.; Fu, L.; Peng, R.; Wen, X.; Chen, Z.; Liu, Z.; Qin, G. High-performance single CdS nanowire (nanobelt) Schottky junction solar cells with Au/graphene Schottky electrodes. *ACS Appl. Mater. Interfaces* **2010**, *2*, 3406−3410.

(23) Zhang, L.; Li, X.; Mu, Z.; Miao, J.; Wang, K.; Zhang, R.; Chen, S. A novel composite of CdS nanorods growing on a polyaniline-Cd^{2+} particles surface with excellent formaldehyde gas sensing properties at low temperature. *RSC Adv.* **2018**, *8*, 30747−30754.

(24) Bai, H.; Guo, H.; Tan, Y.; Wang, J.; Dong, Y.; Liu, B.; Xie, Z.; Guo, F.; Chen, D.; Zhang, R.; Zheng, Y. Facile synthesis of

mesoporous CdS/PbS/SnO_2 composites for high-selectivity H_2 gas sensor. *Sens. Actuators, B* **2021**, *340*, 129924.
(25) Srinivasan, P.; Jeyaprakash, B. G. Fabrication of highly selective formaldehyde sensor through a novel spray deposited ZnO/CdS heterostructured interface: A surface charge enhancement approach. *J. Alloys Compd.* **2018**, *768*, 1016−1028.
(26) Garcia, L. V.; Mendivil, M. I.; Garcia Guillen, G.; Aguilar Martinez, J. A.; Krishnan, B.; Avellaneda, D.; Castillo, G. A.; Das Roy, T. K.; Shaji, S. CdS thin films prepared by laser assisted chemical bath deposition. *Appl. Surf. Sci.* **2015**, *336*, 329−334.
(27) Li, J.; Lu, Y.; Ye, Q.; Cinke, M.; Han, J.; Meyyappan, M. Carbon Nanotube Sensors for Gas and Organic Vapor Detection. *Nano Lett.* **2003**, *3*, 929−933.
(28) Dua, V.; Surwade, S. P.; Ammu, S.; Agnihotra, S. R.; Jain, S.; Roberts, K. E.; Park, S.; Ruoff, R. S.; Manohar, S. K. All-organic vapor sensor using inkjet-printed reduced graphene oxide. *Angew. Chem., Int. Ed.* **2010**, *49*, 2154−2157.
(29) Zhang, N.; Ma, X.; Han, J.; Ruan, S.; Chen, Y.; Zhang, H.; Li, C. Synthesis of sea urchin-like microsphere of CdS and its gas sensing properties. *Mater. Sci. Eng., B* **2019**, *243*, 206−213.
(30) Zhu, L.; Feng, C.; Li, F.; Zhang, D.; Li, C.; Wang, Y.; Lin, Y.; Ruan, S.; Chen, Z. Excellent gas sensing and optical properties of single-crystalline cadmium sulfide nanowires. *RSC Adv.* **2014**, *4*, 61691−61697.
(31) Tin, A. G.; Bakar, M. Z. A.; Chen, C. M. Detection of ethanol vapours using titanium dioxide (TiO_2) catalytic pellet by conventional and modified sol gel dip-coating Method. *Pertanika J. Sci. Technol.* **2013**, *21*, 327−334.
(32) Lei, Q.; Li, H.; Zhang, H.; Wang, J.; Fan, W.; Cai, L. Three-dimensional hierarchical CuO gas sensor modified by Au nanoparticles. *J. Semiconduct.* **2019**, *40*, 17−23.
(33) Liu, X.-H.; Yin, P.-F.; Kulinich, S. A.; Zhou, Y.-Z.; Mao, J.; Ling, T.; Du, X.-W. Arrays of Ultrathin CdS Nanoflakes with High-Energy Surface for Efficient Gas Detection. *ACS Appl. Mater. Interfaces* **2017**, *9*, 602−609.
(34) Fu, X.; Liu, J.; Wan, Y.; Zhang, X.; Meng, F.; Liu, J. Preparation of a leaf-like CdS micro-/nanostructure and its enhanced gas-sensing properties for detecting volatile organic compounds. *J. Mater. Chem. C* **2012**, *22*, 17782−17791.
(35) Li, S.-H.; Chu, Z.; Meng, F.-F.; Luo, T.; Hu, X.-Y.; Huang, S.-Z.; Jin, Z. Highly sensitive gas sensor based on SnO_2 nanorings for detection of isopropanol. *J. Alloys Compd.* **2016**, *688*, 712−717.
(36) Yang, K.; Ma, J.; Qiao, X.; Cui, Y.; Jia, L.; Wang, H. Hierarchical Porousporous $LaFeO_3$ nanostructure for efficient trace detection of formaldehyde. *Sens. Actuators, B* **2020**, *313*, 128022.
(37) Mirzaei, A.; Kim, J.-H.; Kim, H. W.; Kim, S. S. How shell thickness can affect the gas sensing properties of nanostructured materials: Survey of literature. *Sens. Actuators, B* **2018**, *258*, 270−294.
(38) Qiao, X.; Xu, Y.; Yang, K.; Ma, J.; Li, C.; Wang, H.; Jia, L. Mo doped $BiVO_4$ gas sensor with high sensitivity and selectivity towards H_2S. *Chem. Eng. J.* **2020**, *395*, 125144.
(39) Chu, X.; Chen, T.; Zhang, W.; Zheng, B.; Shui, H. Investigation on formaldehyde gas sensor with ZnO thick film prepared through microwave heating method. *Sens. Actuators, B* **2009**, *142*, 49−54.
(40) Zhang, J.; Lu, H.; Zhang, L.; Leng, D.; Zhang, Y.; Wang, W.; Gao, Y.; Lu, H.; Gao, J.; Zhu, G.; Yang, Z.; Wang, C. Metal−organic framework-derived ZnO hollow nanocages functionalized with nanoscale Ag catalysts for enhanced ethanol sensing properties. *Sens. Actuators, B* **2019**, *291*, 458−469.
(41) Dhakshinamoorthy, J.; Pullithadathil, B. New Insights Towards Electron Transport Mechanism of Highly Efficient p-Type CuO (111) Nanocuboids-Based H_2S Gas Sensor. *J. Phys. Chem. C* **2016**, *120*, 4087−4096.
(42) Xiao, L.; Shu, S.; Liu, S. A facile synthesis of Pd-doped SnO_2 hollow microcubes with enhanced sensing performance. *Sens. Actuators, B* **2015**, *221*, 120−126.
(43) Xu, K.; Yang, Y.; Yu, T.; Yuan, C. WO_3 Nanofibers Anchored by Porous $NiCo_2O_4$ Nanosheets for Xylene Detection. *Ceram. Int.* **2018**, *44*, 21717−21724.
(44) Geng, W.; Ma, Z.; Zhao, Y.; He, X.; Duan, L.; Tu, J.; Zhang, Q. The self-assembly of octahedral Cu_xO and its triethylamine-sensing properties. *Sens. Actuators, B* **2020**, *312*, 128014.
(45) Cai, Z.; Park, S. Enhancement mechanisms of ethanol-sensing properties based on Cr_2O_3 nanoparticle-anchored SnO_2 nanowires - ScienceDirect. *J. Mater. Res. Technol.* **2020**, *9*, 271−281.
(46) Giberti, A.; Casotti, D.; Cruciani, G.; Fabbri, B.; Gaiardo, A.; Guidi, V.; Malagù, C.; Zonta, G.; Gherardi, S. Electrical conductivity of CdS films for gas sensing: Selectivity properties to alcoholic chains. *Sens. Actuators, B* **2015**, *207*, 504−510.
(47) Wang, Z.; Yang, X.; Jia, H.; Wang, Y. Preparation of self-assembled hollow microsphere CdS via solvothermal method and its optical properties. *J. Mater. Sci.: Mater. Electron.* **2016**, *27*, 9725−9733.

https://doi.org/10.1021/acsomega.1c06211
ACS Omega 2022, 7, 1468−1476